Design of a β-Ga_2O_3 Schottky Barrier Diode With p-Type III-Nitride Guard Ring for Enhanced Breakdown

Saurav Roy, Arkka Bhattacharyya, and Sriram Krishnamoorthy, *Member, IEEE*

***Abstract*— This work presents the electrostatic analysis of a novel Ga_2O_3 vertical Schottky diode with three different guard ring (GR) configurations to reduce the peak electric field at the metal edges. Highly doped p-type GaN, p-type nonpolar AlGaN, and polarization-doped graded p-AlGaN are simulated and analyzed as the GR material, which forms a heterojunction with the Ga_2O_3 drift layer. GR with nonpolar graded p-AlGaN with a bandgap larger than Ga_2O_3 is found to show the best performance in terms of screening the electric field at the metal edges. The proposed GR configuration is also compared with a reported Ga_2O_3 Schottky diode with no GR and a structure with high-resistive nitrogen-doped GR. The optimized design is predicted to have a breakdown voltage as high as 6.2 kV and a specific ON-resistance of 3.55 mΩ-cm^2, which leads to an excellent power figure of merit of 10.8 GW/cm^2.**

***Index Terms*— AlGaN, Ga_2O_3, GaN, guard ring (GR), polarization doping, Schottky barrier diode (SBD), TCAD simulation.**

I. Introduction

GALLIUM oxide (Ga_2O_3) has a huge potential for power device applications due to its high breakdown field. β-Ga_2O_3 has a bandgap (4.6 eV) larger than GaN and SiC, with an estimated critical breakdown field as high as 8 MV/cm. Due to the large critical electric field, the Baliga figure of merit (BFOM) relevant to power switching could be 2000–3400 times that of Si, which is several times larger than that of SiC or GaN. Low-doped drift layers in conjunction with large bandgap materials can enable very high breakdown voltage. Various power devices using β-Ga_2O_3 have been demonstrated recently with high breakdown voltage in the vertical geometry. [1]–[12].

Several field management techniques have been explored for Schottky diodes over the years, which includes edge terminations, superjunctions, and so on. Guard ring (GR) is one such edge termination technique where the anode metal edge is surrounded by a doped region with opposite polarity to that of the drift region to screen the high electric field generated at the metal edge. Lin *et al.* [13] recently demonstrated a Schottky barrier diode (SBD) with nitrogen ion-implanted GR with a maximum breakdown voltage of 1.43 kV. Zhou *et al.* [14] also demonstrated a Ga_2O_3 SBD using Mg ion-implanted GR with a breakdown voltage of 1.65 kV. A similar design with argon-implanted edge termination has also been reported by Gao *et al.* [15]. Although these devices can achieve a breakdown improvement compared with the case with no GRs, the lack of electric field screening due to the absence of a quasi-neutral region in the GR limits the breakdown voltage. A high-resistive GR, as demonstrated in the previous devices, can spread the depletion region and reduce the field crowding at the metal edges. However, a GR with a quasi-neutral region can be very effective in screening the electric field at the metal edges due to the presence of a quasi-neutral region and can dramatically shift the high field region from the metal edge to deep inside the device, thereby eliminating the effect of surface states, which causes a premature breakdown. Because of the absence of a shallow acceptor in β-Ga_2O_3, p-doped III-nitrides would be a viable option for GR material to get a quasi-neutral region. The idea of heterostructure GRs has been proposed on the silicon carbide substrate previously [16]. Muhammed *et al.* [17] have reported the growth of *c*-plane n-GaN epilayer on ($\bar{2}$ 0 1) β-Ga_2O_3 substrate using metal–organic chemical vapor deposition (MOCVD). Vertical blue-LEDs have also been demonstrated on ($\bar{2}$ 0 1) β-Ga_2O_3 substrates [18]. Shimamura *et al.* [19] reported the growth of *c*-plane GaN on (1 0 0)-oriented β-Ga_2O_3 substrate using MOCVD. On the other hand, Cao *et al.* [20] reported the growth of nonpolar *a*-plane GaN on (0 1 0)-oriented β-Ga_2O_3 substrate by MOCVD. All these reports confirm the viability of growing electronic grade polar and nonpolar GaN on β-Ga_2O_3 substrates depending on the choice of the orientation of the substrate.

In this article, we propose and design a Ga_2O_3 SBD with a p-doped III-nitride GR using electric field simulations. We have explored three GR configurations: 1) p-gallium nitride (p-GaN) GR; 2) nonpolar graded p-aluminum gallium nitride (p-AlGaN) GR; and 3) a polar graded p-AlGaN GR. In this work, we perform detailed electrostatic simulations to capture and manage high electric fields in III-nitride/β-Ga_2O_3

Manuscript received June 26, 2020; revised August 16, 2020 and September 12, 2020; accepted September 16, 2020. Date of publication October 6, 2020; date of current version October 22, 2020. This work was supported by the Air Force Office of Scientific Research under Award FA9550-18-1-0507 (Program Manager: Dr. Ali Sayir) and by the National Science Foundation (NSF) under Grant DMR-1931652. Any opinions, findings, and conclusions or recommendations expressed in this material are those of the author(s) and do not necessarily reflect the views of the United States Air Force. The review of this article was arranged by Editor S. Chowdhury. *(Corresponding author: Saurav Roy.)*

The authors are with the Department of Electrical and Computer Engineering, The University of Utah, Salt Lake City, UT 84112 USA (e-mail: u1268405@utah.edu; a.bhattacharyya@utah.edu; sriram.krishnamoorthy@utah.edu).

Color versions of one or more of the figures in this article are available online at http://ieeexplore.ieee.org.

Digital Object Identifier 10.1109/TED.2020.3025268

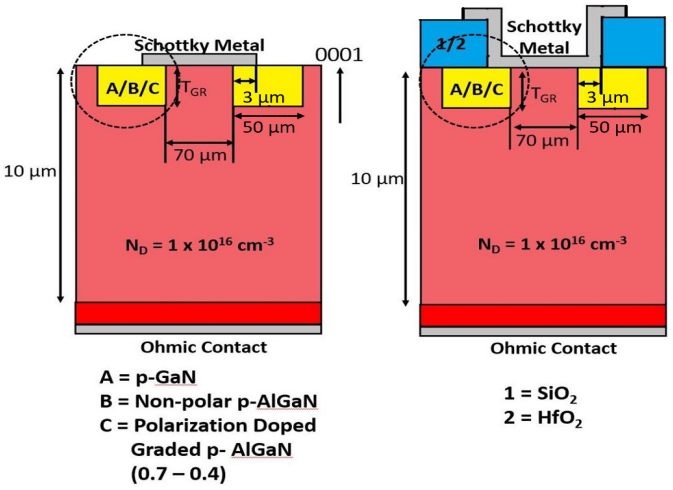

Fig. 1. Schematic of Ga_2O_3 SBD with GRs where (A) Nonpolar p-GaN GR, (B) Nonpolar p-AlGaN GR, (C) Polarization-doped graded p-AlGaN GR with: 1) SiO_2 and 2) HfO_2 as field plate oxide.

heterostructures. The design is optimized to extract the optimum device parameters, which efficiently reduces the electric field. We have also explored the additional use of the field plate in the aforementioned optimum design to further minimize the peak electric field in the device structure.

II. Simulation Methodology

The SBD device structure (see Fig. 1) with varied GR thickness of T_{GR}, a 10-μm-thick drift layer ($N_D = 10^{16}$ cm^{-3}), Ni/Au Schottky metal with a barrier height Φ_B of 1.4 eV [24], and a Schottky metal GR overlap of 3 μm is simulated using Sentaurus [25] 2-D TCAD device simulator. The width of the GR is considered to be 50 μm. In the simulation, adequate numerical convergence was reached by an optimized meshing, with fine grid spacing for the key electrical layers and their interfaces and larger spacings for the drift region. The spontaneous polarization model is used to include a polarization effect in the case of graded polar p-AlGaN. The spontaneous polarization values of -0.034 and -0.09 C/m^2 are considered for GaN and AlN [23]. For p-type doping in GaN and AlGaN, an incomplete ionization model is also used to reflect the accurate hole concentration. In order to capture the accurate results for the high doping case, the Fermi–Dirac model is included for device operating biases. The device simulation setup uses a well-calibrated mobility model and thermodynamic transport model to match the recent experimental results [13]. The device breakdown voltage can be extracted from E-field simulation when the peak E-field reaches the GaN (3.3 MV/cm) or Ga_2O_3 (8 MV/cm) critical E-field. Band offsets were determined using the electron affinity rule. The GaN/Ga_2O_3 band offset estimated using electron affinity rule matches well with the experimentally determined band offsets [26]. The ionization integrals for avalanche breakdown were not evaluated in order to avoid excessive computation time. Furthermore, accurate ionization rate parameters are currently unknown for Ga_2O_3. Hence, it should be noted that the breakdown is not directly calculated but can be estimated

TABLE I
Material Parameters

Material	Ga_2O_3	GaN	AlN
Bandgap (eV)	4.85 [21]	3.3 [22]	6.2 [22]
Electron affinity (eV)	3.9 [21]	3.9 [22]	0.6 [22]
Relative permittivity	10 [21]	8.9 [23]	8.5 [23]
Electron Effective mass	$0.28m_0$	$0.22m_0$	$0.4m_0$
Hole Effective mass	-	$1m_0$	$4m_0$
Critical Electric Field (MV/cm)	8 [21]	3.3 [23]	15 [23]
Sn Activation energy (eV)	0.03 [21]	-	-
Mg Activation energy (eV)	-	0.2 [23]	0.6 [23]
Spontaneous Polarization (C/m^2)	-	-0.034	-0.09

based on the generated electric field distributions [27]–[29]. It should also be noted that, in real devices, field crowding can also occur in the device corners. However, those fields are always lower than the field crowding at the electrode edges, which is the primary cause of device breakdown. Hence, our comparison of device breakdown for the various configurations based on 2-D simulation is considerably reliable and was also demonstrated by other works [27]. All the material parameters for β- Ga_2O_3, GaN, and AlN assumed in the device simulation are presented in Table I. All the other material parameters for intermediate Al compositions in $Al_xGa_{1-x}N$ have been calculated based on GaN and AlN parameters using Vegard's law.

III. Results and Discussion

The SBD with nitrogen-doped GR and the one with no GR are simulated for comparison, and the electric field profiles are shown in Fig. 2(a) (i) and (ii), respectively. The circled cross section in Fig. 1 is magnified and shown for all the electric field contours. The bias voltage is taken to be 1500 V. Ionization energy of nitrogen in β-Ga_2O_3 is considered to be 2 eV [30]. The maximum electric field is at the metal edge in both the cases, and we can see that the field is reduced in the GR structure in Fig. 2(b) as expected and also experimentally reported [13].

We now explore the use of nonpolar p-GaN as the GR material [see Fig. 3(a)]. The use a of magnesium-doped GaN GR enables screening of the electric field at the metal edges due to the presence of a quasi-neutral region. The activation energy for Mg in the case of p-GaN is considered to be 0.2 eV [31]. The doping concentration is taken to be 10^{20} cm^{-3} (hole concentration $= 8.2\times$ 10^{18} cm^{-3}), the GR thickness is 0.5 μm, and the anode voltage is 2000 V. The peak electric field has now moved to the p-GaN/n-Ga_2O_3 heterojunction as can be seen in the electric field contour shown in Fig. 3(a). Fig. 3(b) shows the equilibrium energy band diagram of p-GaN/n-Ga_2O_3 heterojunction. At the anode bias of 2000 V, the peak electric field at the p-GaN/n-Ga_2O_3 heterojunction exceeds the critical field of GaN (3.3 MV/cm). We simulated the p-GaN GR configuration as a function of anode voltage, and the results are presented in Fig 5. The breakdown voltage of the p-GaN GR configuration presented here is 750 V.

To be able to leverage the high critical E-field of β-Ga_2O_3, a better design would be to use a GR material with an enhanced critical field compared with β-Ga_2O_3. Thus, we now study a graded p-AlGaN GR with aluminum composition

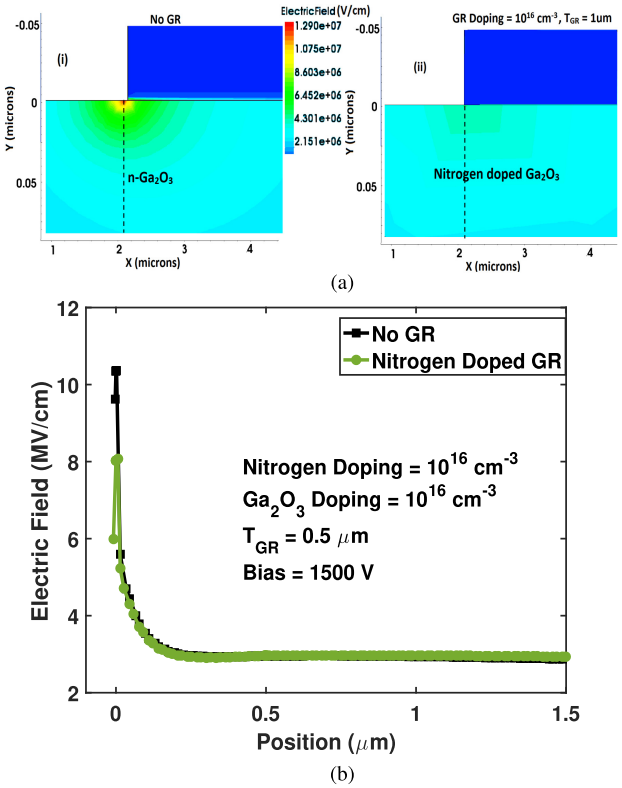

Fig. 2. (a) Electric field distribution in SBD for (i) no GR (ii) Nitrogen-doped GR at bias voltage of 1500 V. (b) Electric field versus position for N-doped GR and no GR at 1500 V along the cutlines shown in the contour plots.

graded from 70% at the AlGaN/Ga_2O_3 interface to 40% at the SBD surface. Fig. 3(c) shows the electric field distribution using graded AlGaN for a doping concentration of 10^{20} cm^{-3}. However, since the ionization energy of Mg is very high for AlGaN with high Al composition, it is very difficult to realize a high hole concentration. In fact, for Mg concentration below 10^{18} cm^{-3}, the peak electric field is always at the metal edge because of the depletion of the entire GR. However, if we grow *c*-axis-oriented AlGaN with graded Al composition with decreasing Al composition from heterointerface to the surface, we can realize a 3-D slab of holes (3DHS) [32] due to the polarization doping effect. Fig. 3(e) shows the electric field distribution in the polarization-doped p-$Al_xGa_{(1-x)}N$ (where $x = 70\%$ at the heterojunction to 40% at the SBD surface) GR. The hole concentration in this GR structure is increased from the nonpolar case by a significant amount ($2\times$ 10^{17} to $6\times$ 10^{18} cm^{-3}). The band diagram of the polarization-doped polar graded p-AlGaN GR configuration is shown in Fig. 3(f). It can be observed that the peak electric field is now at the heterojunction mainly due to the positive polarization sheet charge at the p-$Al_{0.7}Ga_{0.3}N$/n-Ga_2O_3 heterojunction. The energy bands fall rapidly at the polar p-AlGaN/n-Ga_2O_3 interface, thus increasing the electric field compared with the nonpolar p-AlGaN/n-Ga_2O_3 interface, as shown in Fig. 3(g). Even for the low-doped case, the bands fall rapidly at the p-AlGaN/n-Ga_2O_3 heterointerface, as shown in Fig. 4. Thus, a polarization-doped p-AlGaN GR would serve no benefit in reducing the peak electric field.

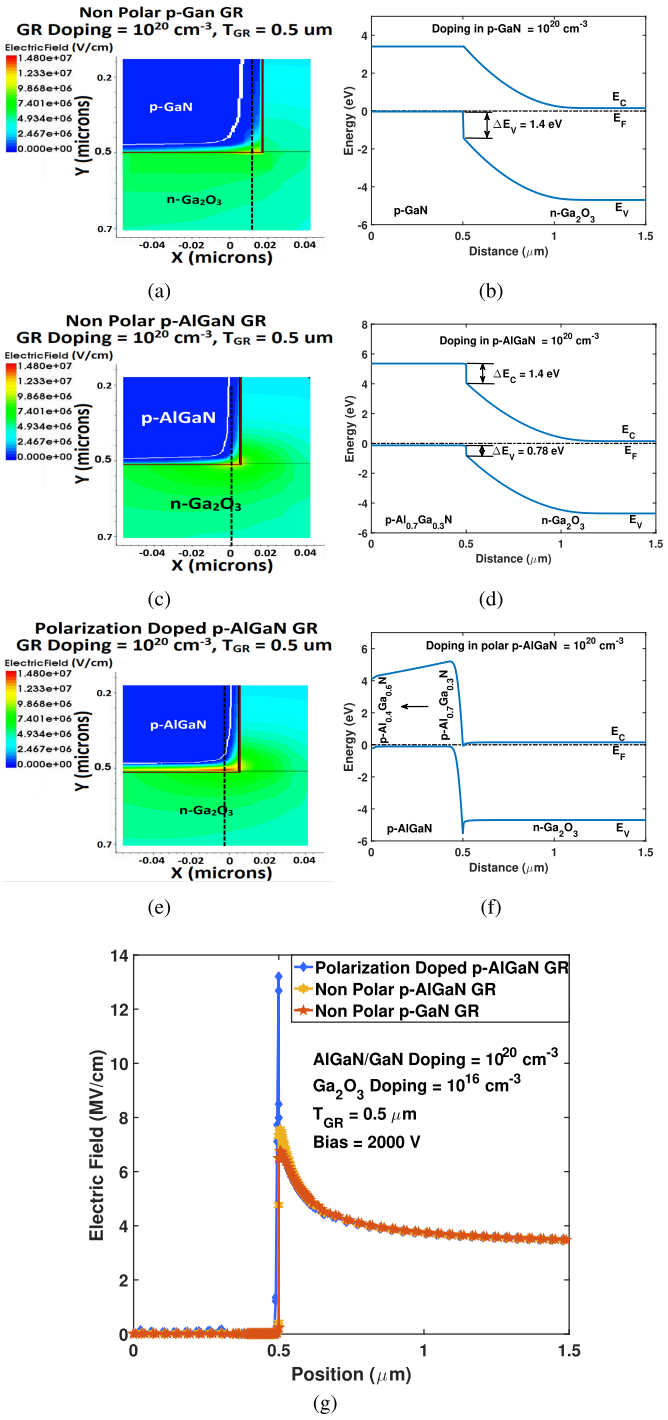

Fig. 3. Electric field distribution and equilibrium energy band diagram for SBD with (a) and (b) nonpolar p-GaN GR, (c) and (d) nonpolar p-AlGaN GR, and (e) and (f) polarization-doped p-AlGaN GR, respectively, at bias voltage of 2000 V and GR doping of 10^{20} cm^{-3}. (g) Electric field versus position in SBD for the three different GR at 2000 V and at GR doping of 10^{20} cm^{-3} along the cutlines shown in the contour plots.

Fig. 5 shows the peak electric field versus applied bias for SBD with the six different GR structures. The doping concentration for p-type GR is taken to be of 10^{20} cm^{-3}, and for nitrogen-doped case, it is taken to be of 10^{16} cm^{-3}, and the GR thickness is taken to be 0.5 μm. The nonpolar graded p-AlGaN, ungraded p-AlGaN, and p-GaN GR show the best performance in terms of reducing the peak electric field.

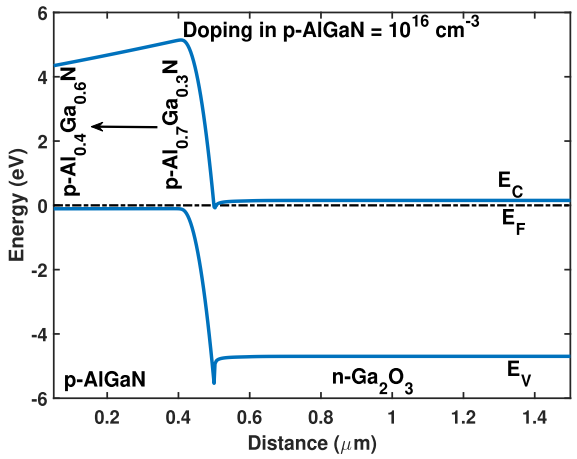

Fig. 4. Equilibrium energy band diagram of the simulated SBD with polarization-doped p-AlGaN GR for $T_{GR} = 0.5\ \mu$m and $N_D = 10^{16}$ cm^{-3}. Al composition is graded from 70% to 40% from the p-AlGaN/n-Ga_2O_3 heterointerface to the SBD surface.

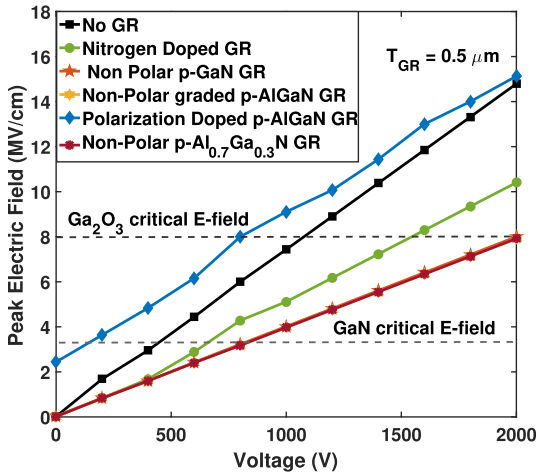

Fig. 5. Peak electric field versus applied bias in SBD for different GR configurations with 0.5 μm of GR thickness and 10^{20} cm^{-3} of GR doping.

However, the SBD with GaN GR crosses its critical electric field of 3.3 MV/cm at 750 V. The nonpolar p-$Al_xGa_{1-x}N$ GR with uniform Al composition ($x = 70\%$) has a critical electric field as high as gallium oxide, and hence, the breakdown voltage can be as high as 2000 V, as shown in the Fig. 5. The electric field is very high in the case of the SBD with polarization-doped AlGaN GR because of the high field at the heterointerface.

Doping and thickness of the GR are critical parameters that would determine the amount of electric field screening and location of the peak electric field. We simulated the three GR configurations excluding the SBD with no GR and nitrogen-doped GR, as a function of Mg doping for a fixed thickness of 0.5 μm at a bias of 2000 V. Doping in the GR is found to determine the location of the peak electric field, as shown in Fig. 6. For the polar p-AlGaN GR, the peak electric field is always at the heterojunction irrespective of the doping. In the case of p-GaN and nonpolar p-AlGaN GR, the peak field is at the metal edge for doping concentrations lower than 10^{18} cm^{-3}. Since a high GR doping is not necessary to minimize the peak field at the metal edge, and nonpolar graded and ungraded p-AlGaN GR shows similar performance,

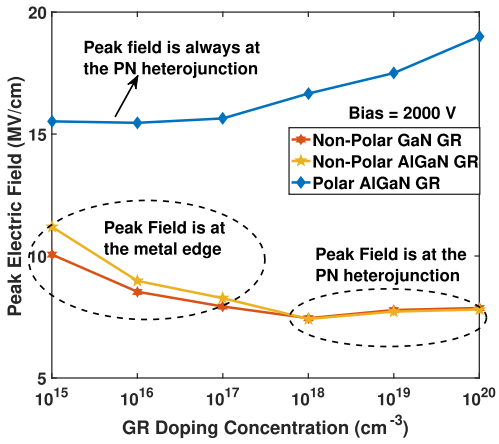

Fig. 6. Peak electric field versus GR doping concentration with 0.5 μm of GR thickness and at applied bias of 2000 V for different GR configurations.

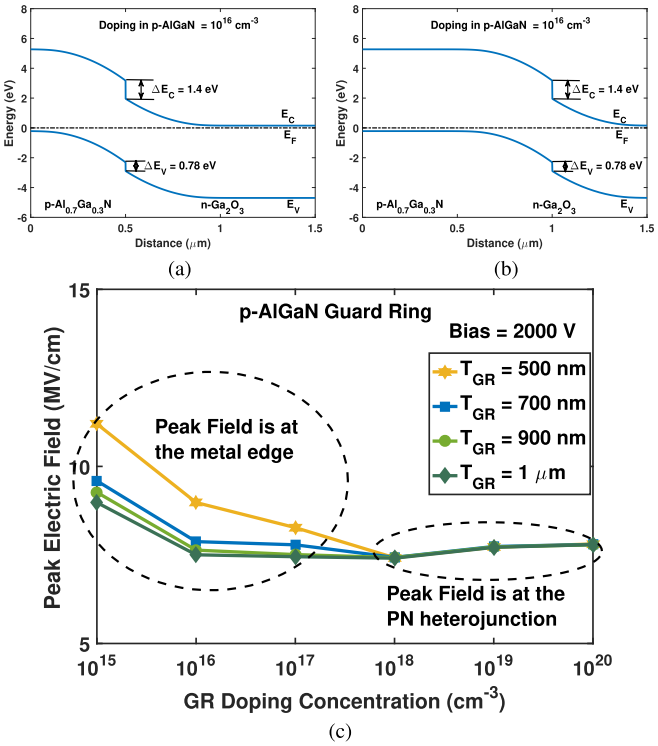

Fig. 7. Equilibrium energy band diagram of the simulated SBD with nonpolar p-AlGaN GR for (a) $T_{GR} = 0.5\ \mu$m and (b) $T_{GR} = 1\ \mu$m. Al composition is considered to be 70%. (c) Peak electric field versus GR doping concentration with nonpolar AlGaN GR and at applied bias of 2000 V for different GR thicknesses.

compositional grading in the GR is not required, which will mitigate the challenge involving the growth of the graded epitaxial layer of AlGaN inside the pocket of Ga_2O_3.

The electric field simulations clearly establish the comparably superior performance of nonpolar p-AlGaN GR configuration. We now further focus on this particular configuration and study the effect of the thickness of the GR. In the case of low-doped GRs, in order to take advantage of a quasi-neutral region, it is essential that the thickness must be sufficiently large to realize an undepleted region close to the metal. The equilibrium energy band diagram of nonpolar graded p-AlGaN GR with low doping (10^{16} cm^{-3}) with two different thicknesses is shown in Fig. 7(a) and (b). The presence of

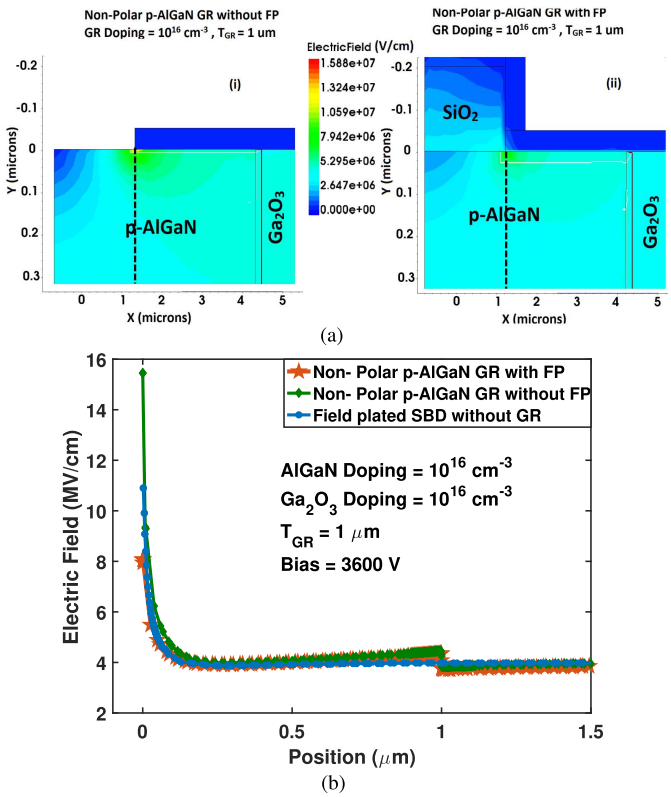

Fig. 8. (a) Electric field distribution in SBD for 1-μm-thick nonpolar AlGaN GR (i) without field plate (ii) with field plate at bias voltage of 3600 V and GR doping of 10^{16} cm^{-3}. (b) Electric field versus position for the two GR structure and also for field plated SBD with no GR at 3600 V and at GR doping of 10^{16} cm^{-3} along the cutlines shown in the contour plots.

a quasi-neutral region near the metal by employing a thick low-doped GR [see Fig. 7(b)] is expected to be beneficial for electric field screening. The quasi-neutral region near the metal edge provides room for the growth of the depletion region at high reverse bias. The effect of GR thickness as a function of Mg doping is summarized in Fig. 7(c). The peak electric field at a bias of 2000 V can be reduced from 9 to 7.5 MV/cm at a GR doping of 10^{16} cm^{-3}. The peak electric field reduces as the doping increases for doping concentration less than 10^{18} cm^{-3}. As the GR thickness increases, the peak electric field reduces till a doping concentration of 10^{17} cm^{-3}. Above this concentration, the peak electric field shifts to the p-n heterojunction, and the GR thickness has no effect on the peak electric field. In this regime, there is no advantage of using a field plate since the peak field region is buried.

To further improve electric field management, we choose GR configuration B with a thickness of 1 μm and a doping concentration of 10^{16} cm^{-3}. In this case, the peak electric field is at the metal edge. Now, we analyze the potential for further improvement in the breakdown voltage with a field plate. Fig. 8(a) shows the electric field distribution in the SBD for a GR thickness of 1 μm and at a bias voltage of 3600 V: 1) without and 2) with a field plate, respectively. An SiO_2 layer of 200 nm is used as the field plate oxide. We also compared our design with a field plated SBD without GR, as shown in 8(b). The field plating has more impact on the reduction of the peak electric field compared with the SBD

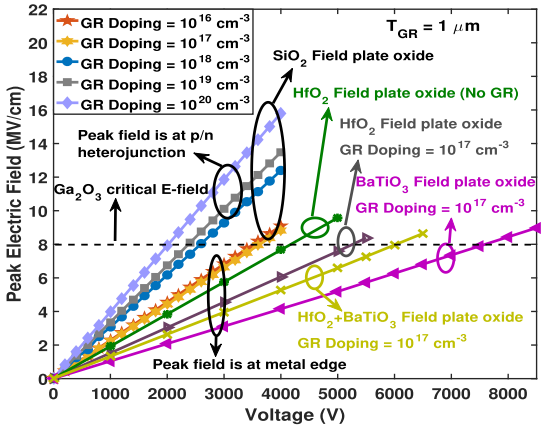

Fig. 9. Peak electric field versus applied bias in SBD with field plate and nonpolar AlGaN GR for different GR doping concentrations and with field plate oxides with different dielectric constants. Also, compared with standard field plated SBD structure with no GR.

with only GR. However, field-plated SBD combined with a thick p-AlGaN GR dramatically reduces the peak electric field at the metal edge. Here again, the peak electric field reduces as the doping increases till a doping concentration of 10^{17} cm^{-3}. Thus, the best design would be a thick low-doped p-AlGaN GR with a field plate.

Fig. 9 shows the effect of field plating on reducing the peak electric field for the SBD with nonpolar p-AlGaN GR. In Fig. 9, we can see that, for doping concentration less than 10^{18} cm^{-3}, in the case of nonpolar p-AlGaN GR, field plating significantly reduces the electric field at the metal edge, and the electric field crosses the β-Ga_2O_3 critical electric field of 8 MV/cm at a bias voltage of around 3600 V. For doping concentration above 10^{17} cm^{-3}, the field plating has no effect on reducing the electric field because of shifting of the peak electric field from metal edge to the p-n heterojunction. We can also see that the use of a high-k dielectric (HfO_2, in this case, with relative permittivity of 22) with the same dimension as the previous case as field plate oxide in conjunction with the GR reduces the peak electric field dramatically, and the device reaches the β-Ga_2O_3 critical electric field of 8 MV/cm at a reverse bias voltage of 5200 V, which is significantly higher than the highest reported breakdown voltage for any vertical SBD with 10-μm drift layer [33]. The high permittivity difference between the semiconductor and the dielectric generates polarization bound charge inside the dielectric, which balances the depletion charge at the semiconductor interface [29], [34], [35]. This charge balance results in flattening of the electric field profile at the dielectric/semiconductor interface, reducing its peak magnitude. We have also simulated a field plated SBD with HfO_2 as field plated oxide without a GR, and it achieves a breakdown voltage of 4300 V. Thus, the use of a GR in conjunction with a field plate increases the breakdown voltage by 900 V compared with the field plated SBD with no GR. We have also analyzed other extreme high-k material, such as $BaTiO_3$ (relative permittivity of 300) as field plate oxide, and the breakdown voltage was found to reach 7800 V when used in conjunction with GR. Since $BaTiO_3$ has no conduction

band offset with β-Ga_2O_3, the use of $BaTiO_3$ underneath the metal might cause charge trapping inside the dielectric layer. To mitigate the charge trapping, we have analyzed a stacked dielectric of HfO_2 (5 nm)+$BaTiO_3$ (295 nm). During forward conduction, when electron flows from the cathode to the anode Schottky metal, the presence of a conduction band offset at the dielectric/Ga_2O_3 interface could potentially block the current flow through the dielectric, which can also potentially prevent bulk electron trapping in the dielectric. Here, the large thickness ratio is used to maintain the high dielectric constant for the series configuration, which results in an effective dielectric constant of 248. Using this structure in conjunction with the thick GR, we are able to get a breakdown voltage of 6200 V.

Among all the devices described, the SBD with nonpolar p-AlGaN GR added with field plate and a high-k field plate oxide is found out to be the best choice to reduce the electric field. The thick β-Ga_2O_3 epilayers ($\sim$10 μm) on (010) β-Ga_2O_3 substrates used in this design can be grown using halide vapor phase epitaxy (HVPE) and has already been demonstrated [36], [37]. Selective area epitaxy of AlGaN GRs inside Ga_2O_3 trench pockets can be done using MOCVD [38], [39]. We understand AlGaN heteroepitaxy on Ga_2O_3 could lead to compromised material quality and will require extensive growth and process optimizations. Experimentally, trench Ga_2O_3 SBDs with field plate structures were able to achieve a figure of merit (FOM) as high as 0.95 GW/cm^2 [33]. Using the concepts explored in this work, if Ga_2O_3 SBDs with GR in conjunction with field plates are implemented, we expect this design to surpass the already high FOM achieved with Ga_2O_3 power SBDs. For instance, with a breakdown voltage of 6200 V and an estimated $R_{ON,SP}$ of 3.55 mΩ-cm^2, assuming a mobility of 176 cm^2/V·s [40], we should be able to achieve extremely high FOM of 10.8 GW/cm^2.

IV. Conclusion

A novel approach to reduce the electric field and, thus, increasing the breakdown voltage for SBD by using p-doped III-nitride GR is proposed and shown through a detailed device simulation. This approach circumvents the issue of lack of p-type doping in gallium oxide. The SBD with thick low-doped nonpolar p-AlGaN GR in conjunction with a field plate and a high-k dielectric can serve best in terms of reducing the peak electric field. The inclusion of field plate and a high permittivity field plate oxide in the case of low-doped GR is shown to further reduce the electric field at the metal edges. Further research into the interface properties of the AlGaN/Ga_2O_3 heterointerface will lead to better understanding and the use of such heterojunction-based structures for high-performance power electronic devices.

Acknowledgment

This material is based upon work supported by the Air Force Office of Scientific Research under Award Number FA9550-18-1-0507 (Program Manager: Dr. Ali Sayir). Any opinions, findings, and conclusions or recommendations expressed in this material are those of the author(s) and do not necessarily reflect the views of the United States Air Force. The authors also acknowledge funding from the National Science Foundation (NSF) through Grant DMR-1931652.

References

[1] M. Higashiwaki, K. Sasaki, A. Kuramata, T. Masui, and S. Yamakoshi, "Gallium oxide (Ga_2O_3) metal-semiconductor field-effect transistors on single-crystal β-Ga_2O_3 (010) substrates," *Appl. Phys. Lett.*, vol. 100, no. 1, 2012, Art. no. 013504.

[2] K. Sasaki, A. Kuramata, T. Masui, E. G. Villora, K. Shimamura, and S. Yamakoshi, "Device-quality β-Ga_2O_3 epitaxial films fabricated by ozone molecular beam epitaxy," *Appl. Phys. Express*, vol. 5, no. 3, 2012, Art. no. 035502.

[3] K. Sasaki, M. Higashiwaki, A. Kuramata, T. Masui, and S. Yamakoshi, "Ga_2O_3 Schottky barrier diodes fabricated by using single-crystal β-Ga_2O_3 (010) substrates," *IEEE Electron Device Lett.*, vol. 34, no. 4, pp. 493–495, Apr. 2013.

[4] M. Higashiwaki *et al.*, "Ga_2O_3 Schottky barrier diodes with n-Ga_2O_3 drift layers grown by HVPE," in *Proc. 73rd Annu. Device Res. Conf. (DRC)*, 2015, pp. 29–30.

[5] K. Konishi *et al.*, "1-kV vertical Ga_2O_3 field-plated Schottky barrier diodes," *Appl. Phys. Lett.*, vol. 110, no. 10, 2017, Art. no. 103506.

[6] J. Yang *et al.*, "High reverse breakdown voltage Schottky rectifiers without edge termination on Ga_2O_3," *Appl. Phys. Lett.*, vol. 110, no. 19, 2017, Art. no. 192101.

[7] K. Sasaki *et al.*, "First demonstration of Ga_2O_3 trench MOS-type Schottky barrier diodes," *IEEE Electron Device Lett.*, vol. 38, no. 6, pp. 783–785, Jun. 2017.

[8] J. Yang, S. Ahn, F. Ren, S. Pearton, S. Jang, and A. Kuramata, "High breakdown voltage (−201) β-Ga_2O_3 Schottky rectifiers," *IEEE Electron Device Lett.*, vol. 38, no. 7, pp. 906–909, Jul. 2017.

[9] J. Yang, F. Ren, M. Tadjer, S. Pearton, and A. Kuramata, "2300 V reverse breakdown voltage Ga_2O_3 schottky rectifiers," *ECS J. Solid State Sci. Technol.*, vol. 7, no. 5, p. Q92, 2018.

[10] W. Li *et al.*, "1230 V β-Ga_2O_3 trench Schottky barrier diodes with an ultra-low leakage current of < 1 μ A/cm^2," *Appl. Phys. Lett.*, vol. 113, no. 20, 2018, Art. no. 202101.

[11] W. Li *et al.*, "2.44 kV Ga_2O_3 vertical trench Schottky barrier diodes with very low reverse leakage current," in *IEDM Tech. Dig.*, Dec. 2018, pp. 5–8.

[12] Y. Wang *et al.*, "High-voltage (−201) β-Ga_2O_3 vertical Schottky barrier diode with thermally-oxidized termination," *IEEE Electron Device Lett.*, vol. 41, no. 1, pp. 131–134, Jan. 2020.

[13] C.-H. Lin *et al.*, "Vertical Ga_2O_3 Schottky barrier diodes with guard ring formed by nitrogen-ion implantation," *IEEE Electron Device Lett.*, vol. 40, no. 9, pp. 1487–1490, Sep. 2019.

[14] H. Zhou *et al.*, "High-performance vertical β-Ga_2O_3 Schottky barrier diode with implanted edge termination," *IEEE Electron Device Lett.*, vol. 40, no. 11, pp. 1788–1791, Nov. 2019.

[15] Y. Gao *et al.*, "High-voltage β-Ga_2O_3 Schottky diode with argon-implanted edge termination," *Nanosc. Res. Lett.*, vol. 14, no. 1, p. 8, 2019.

[16] Q. Zhang, "Semiconductor devices with heterojunction barrier regions and methods of fabricating same," U.S. Patent 9 117 739, Aug. 25, 2015.

[17] M. Muhammed *et al.*, "High-quality III-nitride films on conductive, transparent (−201) oriented β-Ga_2O_3 using a GaN buffer layer," *Sci. Rep.*, vol. 6, Jul. 2016, Art. no. 29747.

[18] M. M. Muhammed, N. Alwadai, S. Lopatin, A. Kuramata, and I. S. Roqan, "High-efficiency InGaN/GaN quantum well-based vertical light-emitting diodes fabricated on β-Ga_2O_3 substrate," *ACS Appl. Mater. Interfaces*, vol. 9, no. 39, pp. 34057–34063, 2017.

[19] K. Shimamura, E. G. Víllora, K. Domen, K. Yui, K. Aoki, and N. Ichinose, "Epitaxial growth of GaN on (1 0 0) β-Ga_2O_3 substrates by metalorganic vapor phase epitaxy," *Jpn. J. Appl. Phys.*, vol. 44, no. 1L, p. L7, 2004.

[20] Y. Cao, R. Li, A. J. Williams, R. Chu, A. L. Corrion, and R. Chang, "Non-polar GaN film growth on (0 1 0) gallium oxide substrate by metal organic chemical vapor deposition," *J. Mater. Res.*, vol. 32, no. 9, pp. 1611–1617, May 2017.

[21] S. Pearton *et al.*, "A review of Ga_2O_3 materials, processing, and devices," *Appl. Phys. Rev.*, vol. 5, no. 1, 2018, Art. no. 011301.

[22] I. R. Vurgaftman, R. J. Meyer, and L. R. Ram-Mohan, "Band parameters for III-V compound semiconductors and their alloys," *J. Appl. Phys.*, vol. 89, no. 11, pp. 5815–5875, 2001.

[23] M. E. Levinshtein, S. L. Rumyantsev, and M. S. Shur, *Properties of Advanced Semiconductor Materials: GaN, AlN, InN, BN, SiC, SiGe*. Hoboken, NJ, USA: Wiley, 2001.

[24] A. Bhattacharyya *et al.*, "Schottky barrier height engineering in β-Ga_2O_3 using SiO_2 interlayer dielectric," *IEEE J. Electron Devices Soc.*, vol. 8, pp. 286–294, 2020.

[25] *Sentaurus Device User Manual, Version N-2017.09*, Synopsys, Mountain View, CA, USA, Mar. 2017.

[26] W. Wei *et al.*, "Valence band offset of β-Ga_2O_3/wurtzite GaN heterostructure measured by X-ray photoelectron spectroscopy," *Nanosc. Res. Lett.*, vol. 7, no. 1, p. 562, 2012.

[27] M. Xiao, R. Zhang, D. Dong, H. Wang, and Y. Zhang, "Design and simulation of GaN superjunction transistors with 2-DEG channels and fin channels," *IEEE J. Emerg. Sel. Topics Power Electron.*, vol. 7, no. 3, pp. 1475–1484, Sep. 2019.

[28] Y. Zhang *et al.*, "Electrothermal simulation and thermal performance study of GaN vertical and lateral power transistors," *IEEE Trans. Electron Devices*, vol. 60, no. 7, pp. 2224–2230, Jul. 2013.

[29] Z. Xia, C. Wang, N. K. Kalarickal, S. Stemmer, and S. Rajan, "Design of transistors using high-permittivity materials," *IEEE Trans. Electron Devices*, vol. 66, no. 2, pp. 896–900, Feb. 2019.

[30] M. J. Tadjer, J. L. Lyons, N. Nepal, J. A. Freitas, Jr., A. D. Koehler, and G. M. Foster, "Review—Theory and characterization of doping and defects in β-Ga_2O_3," *ECS J. Solid State Sci. Technol.*, vol. 8, no. 7, pp. Q3187–Q3194, 2019.

[31] M. A. Reshchikov, P. Ghimire, and D. O. Demchenko, "Magnesium acceptor in gallium nitride. I. Photoluminescence from Mg-doped GaN," *Phys. Rev. B, Condens. Matter*, vol. 97, no. 20, May 2018, Art. no. 205204.

[32] J. Simon, V. Protasenko, C. Lian, H. Xing, and D. Jena, "Polarization-induced hole doping in wide-band-gap uniaxial semiconductor heterostructures," *Science*, vol. 327, no. 5961, pp. 60–64, Jan. 2010.

[33] W. Li, K. Nomoto, Z. Hu, D. Jena, and H. G. Xing, "Field-plated Ga_2O_3 trench Schottky barrier diodes with a $BV^2/R_{on,sp}$ of up to 0.95 GW/cm^2," *IEEE Electron Device Lett.*, vol. 41, no. 1, pp. 107–110, Jan. 2020.

[34] S. Rajan, Z. Xia, and C. Wang, "Dielectric passivation for electronic devices," U.S. Patent 16 455 736, Jan. 2, 2020.

[35] T. Kabemura, S. Ueda, Y. Kawada, and K. Horio, "Enhancement of breakdown voltage in AlGaN/GaN HEMTs: Field plate plus high-k passivation layer and high acceptor density in buffer layer," *IEEE Trans. Electron Devices*, vol. 65, no. 9, pp. 3848–3854, Sep. 2018.

[36] H. Murakami *et al.*, "Homoepitaxial growth of β-Ga_2O_3 layers by halide vapor phase epitaxy," *Appl. Phys. Express*, vol. 8, no. 1, 2014, Art. no. 015503.

[37] J. H. Leach, K. Udwary, J. Rumsey, G. Dodson, H. Splawn, and K. R. Evans, "Halide vapor phase epitaxial growth of β-Ga_2O_3 and α-Ga_2O_3 films," *APL Mater.*, vol. 7, no. 2, 2019, Art. no. 022504.

[38] D. Kapolnek *et al.*, "Anisotropic epitaxial lateral growth in GaN selective area epitaxy," *Appl. Phys. Lett.*, vol. 71, no. 9, pp. 1204–1206, Sep. 1997.

[39] Y. Kawaguchi, Y. Honda, H. Matsushima, M. Yamaguchi, K. Hiramatsu, and N. Sawaki, "Selective area growth of GaN on Si substrate using SiO_2 mask by metalorganic vapor phase epitaxy," *Jpn. J. Appl. Phys.*, vol. 37, no. 8B, p. L966, 1998.

[40] Y. Zhang *et al.*, "MOCVD grown epitaxial β-Ga_2O_3 thin film with an electron mobility of 176 cm^2/V s at room temperature," *APL Mater.*, vol. 7, no. 2, 2019, Art. no. 022506.